Precise measurement of the cross section of ^{3}He(^{3}He, 2p)^{4}He by using ^{3}He doubly charged beam

Nobuyuki Kudomi,[1] Masataka Komori,[2] Keiji Takahisa,[1] Sei Yoshida,[1]
Kyo Kume,[3] Hideaki Ohsumi,[4] and Takahisa Itahashi[1,*]
[1]*Research Center for Nuclear Physics, Osaka University, Ibaraki, Osaka 567-0047, Japan*
[2]*National Institute of Radiological Sciences, 4-9-1 Anagawa Inageku, Chiba 263-8555, Japan*
[3]*The Wakasa Wan Energy Research Center, Tsuruga, Fukui 914-0192, Japan*
[4]*Faculty of Culture and Education, Saga University, Saga 840-0027, Japan*
(Received 24 June 2003; published 27 January 2004)

The fusion cross section of ^{3}He(^{3}He, 2p)^{4}He at a center of mass energy of 30–50 keV has been measured by using a helium-3 doubly ionized beam at a low-energy high current accelerator facility OCEAN. Free from molecular interference in the beam, the measurement determines the astrophysical S factor with better statistical and systematic errors than previous data. By using singly and doubly charged helium-3 ions, the facility envisages to provide the data from high-energy to Gamow energy regions.

DOI: 10.1103/PhysRevC.69.015802 PACS number(s): 26.65.+t, 25.55.Hp

I. INTRODUCTION

Of the reactions that involved the solar combustion, namely $d+p \rightarrow {}^3\mathrm{He}+\gamma$, ${}^3\mathrm{He} \rightarrow {}^3\mathrm{He} \rightarrow 2p+\alpha$, and ${}^3\mathrm{He}+\alpha \rightarrow {}^7\mathrm{Be}+\gamma$, we have focused on the cross section measurement of the ${}^3\mathrm{He}+{}^3\mathrm{He}$ reaction at an effective energy of $E_{\mathrm{c.m.}}=30-50$ keV. Among many experiments, the only one which has been conducted at or lower than the Gamow energy is the ${}^3\mathrm{He}+{}^3\mathrm{He} \rightarrow 2p+\alpha$ reaction at the LUNA in Gran Sasso laboratory [1,2]. The latter was performed near the Gamow energy, but not in the range $E_{\mathrm{c.m.}}=25-45$ keV due to accelerator limitations that lower voltage could not be applied with a high voltage static accelerator while higher voltage more than 50 kV could be impossible at the LUNA. For a wider energy range $E_{\mathrm{c.m.}}=17.9-342.5$ keV, the experiments done by Krauss *et al.* slightly extended the data over this energy gap [3]. For the nuclear astrophysics discussion, in particular standard solar model or nucleosynthesis, continuous data down to low energy is crucial to deduce the astrophysical S_{33} and S_{34}. Therefore, successive and precise data from around 50 keV–20 keV center of mass energy are needed. For this purpose, we have constructed a low-energy and compact accelerator facility which provides doubly charged ^{3}He ions for the measurement in the region between 50 keV and 20 keV and also singly charged ^{3}He ions in the region less than 25 keV center of mass energy. This is the first report of a series experiments done at our low-energy high current accelerator facility OCEAN. We obtained precise results from 45.3 to 31.2 keV in center of mass energy for the ${}^3\mathrm{He}+{}^3\mathrm{He} \rightarrow 2p+\alpha$ reaction with a doubly charged incident ^{3}He beam. It has the substantial advantage of eliminating the molecular interference in the proton spectra by the ${}^3\mathrm{He}+d$ reaction caused by the incident HD^+ beam.

II. EXPERIMENTAL APPARATUS

The experimental apparatus OCEAN (Osaka University Cosmological Experimental Apparatus for Nuclear Physics) consists of (1) a powerful ion source that provides an intense current of 200 μA for $^3He^{2+}$ at incident energies of 90.6–62.4 keV (more than 1 mA for $^3He^{1+}$ is obtained with a facile operation), (2) low-energy beam transport with good transmission, (3) a windowless gas target and recirculation/purification system, (4) a reliable calorimeter, (5) detectors for reaction identification, and (6) an electronics and data acquisition system based on CAMAC. The layout of the OCEAN is shown in Fig. 1.

A. Ion source and extraction electrodes

An intense ion source that can produce $^3He^{2+}$ ions is essential for the present study. The NANOGUN™, which was obtained from PANTECH, confines high-temperature electrons produced by the electron cyclotron resonance (ECR) and is assembled into an ECR ion source with 10 GHz, 200 W rf generator (model VZX-6383G5, CPI). The original NANOGUN ECR ion source made by PANTECH can provide 40 μA for $^{40}Ar^{8+}$ at 20 kV extraction voltage with a rf power of 60 W. From these data we could easily foresee the possibilities of obtaining $^3He^{1+}$ or $^3He^{2+}$ ion beams of more than 100 μA, although the applied potential at the extraction is not enough to use this ion source for astrophysical applications in a wider energy range. For this purpose, we redesigned the ion source extraction system to meet the ion optical condition for the present windowless gas target. Leroy *et al.* [4] reported an improvement for the analyzed current and beam emittance of $^3He^{1+}$ beam by a system called multielectrodes extraction for CAPRICE-type ECR ion source. It supplied an analyzed current of 2.3 mA of $^3He^{1+}$ giving a transmission of more than 75% in the beam line [4]. Based on several experimental studies and computer simulations we designed and applied a two-electrode extraction system for the NANOGUN ECR ion source [5]. This improves the beam emittance under the influence of a strong space charge force, and second, it moderates the electric field gradient ascribed to high operational voltage. The intermediate electrode has a conic shape nearly parallel to the end surface of the plasma chamber and the final grounded electrode has a

*Electronic address: kudomi@rcnp.osaka-u.ac.jp

 ©2004 The American Physical Society

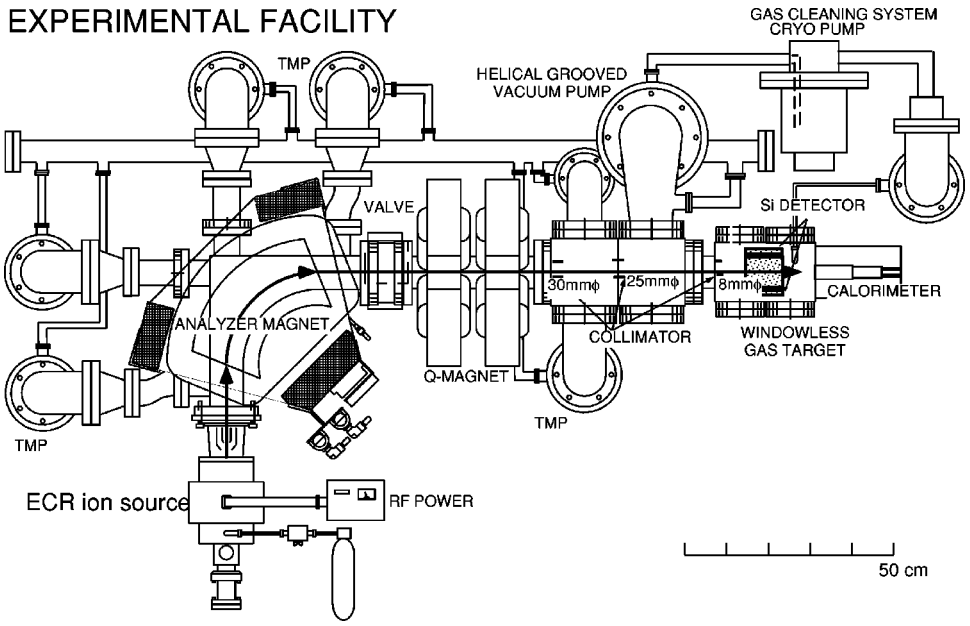

FIG. 1. Complete layout of Osaka University Cosmological Experimental Apparatus for Nuclear Physics, OCEAN.

plane shape with a long straight part. A specially designed ceramic insulator (SUMIKIN CERAMIC Co-Ltd.) with two folds on the surface which has 170 mm in its total length could support up to a 50 kV potential without any surface discharge. The optimization process for applying a suitable voltage to the intermediate electrode progressed considerably during the experiments measured at each center of mass energy. For the present experiment, between 45 keV and 31.2 keV center of mass energy, around 100 μA of doubly charged $^3He^{2+}$ was derived to the gas target. The performance and design have been detailed in previous papers [5].

B. Low-energy beam transport

The low-energy beam transport system between the ECR ion source and the gas target achieved a high beam intensity and other desirable beam qualities, thereby allowing for precision measurements of the present $^3He \rightarrow {}^3He \rightarrow 2p+\alpha$ experiment. Generally, it is known that there is a strong space charge effect in the beam transport at ion currents of more than 1 mA. It is essential that this effect is accounted for when calculating the beam optics. We used a GIOS code developed by Wollnick *et al.* for incorporating this effect [6]. We adopted the *D* (dipole, 90° deflection angle) $+Q+Q$ transport scheme for our system since it is easier to operate with fewer elements. In this calculation we assumed a beam source of 100 π mm mrad emittance and 5 mm in diameter. Despite the variance in the total potential of the beam, a nearly invariant beam could be realized at the source exit using the extraction system stated above. To maintain the minimum slit aperture, we calculated the dimension of the beam at the target position by varying the parameters of elements and drift lengths so as to achieve smaller *dx* (vertical direction) and *dy* (horizontal direction). Very attractive results such as a constant *dx* and *dy* and a nearly parallel beam are shown in Fig. 2. The beam transmission efficiency from the ion source through the target is about 30% (Table I).

C. Windowless gas target

The windowless gas target for the study of the $^3He+{}^3He$ reaction consists of a differential pumping and gas circulation/purification system as shown in Fig. 3.

In order to maintain a pressure of 0.75 Torr in the chamber of the ^3He gas target without a window, the pumping system should be composed of several stages between the

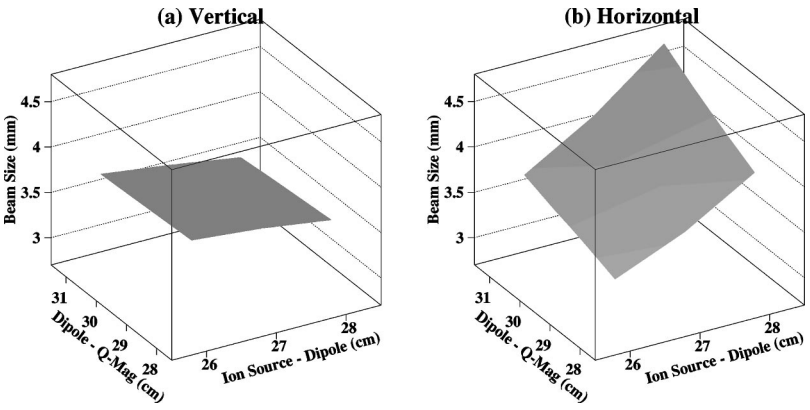

FIG. 2. Beam transport calculation for the present designed scheme consisting of a 90° dipole magnet + quadrupole doublet for 1 mA 50 keV $^3He^{1+}$ beam. The beam size at the target [(a) vertical and (b) horizontal] was calculated as a function of the distance between the ion source to the dipole magnet or dipole magnet to *Q* magnet, respectively. The beam source is assumed to be 100 πmm mrad and 5 mm in diameter.

TABLE I. The achieved beam current at the ion source and the target.

High voltage (H.V.)	(kV)	Target (μA)	Ion source (μA)
40	1^+	1208	3010
	2^+	103	3000
30	1^+	1200	3800
	2^+	35	1900

target chamber and beam transport system. Thus we prepared a helical grooved vacuum pump (model TS-440, OSAKA VACUUM Co.Ltd TS-440) as the main pump for evacuating the gas flow at the viscous region as well as at the higher vacuum region. The collimator sizes at every stage were estimated by calculation in order to maintain a pressure in the range from 1 to 0.01 Torr.

The recirculation system consists of a helium tight pump, an oil-free diaphragm membrane compressor, reservoir vessels, compound gauges, ultrafine regulated valves, and a quadruple mass spectrometer as shown in Fig. 3. Evacuation lines from fore pumps should be connected to the helical grooved vacuum pump in order to secure circulated ^{3}He gas as shown in Fig. 3. Gas flow into the ion source increased the target pressure gradually. Thus, the target pressure was maintained constant by controlling the signal from the capacitance manometer (Barocel-655) located at the target chamber with a gas dosing apparatus (model EVR 116 and RVC 300 controller used in REV mode).

The new purification system developed for the present experiment is quite different from the usual method. It exploits a cryopump (model U-140W, DAIKIN) as a purifier without a special adsorbent and liquid nitrogen, although high heat input could be expected at the high operating pressure. This has been overcome by adding another oil-free turbomolecular pump (model A30FC, ANELVA) between the cryopump and the target chamber. As pointed out by Krauss *et al.* [3], the deuterium contamination both in the target and the beam, resulting from the water vapor, is a crucial problem for obtaining low-energy data, since the $d+{}^3$He reaction cross section is six orders of magnitude higher than that of the ^{3}He+^{3}He reaction [7]. In the case of ${}^3He^{2+}$ beam ($e/m=2/3$), we can avoid molecular interference of the HD^+ beam ($e/m=1/3$) with an analyzer magnet (Fig. 1) contaminating the incident ${}^3He^{1+}$ ($e/m=1/3$) beam, whereas this could not be avoided if we had employed a single charged ^{3}He beam ($e/m=1/3$). We measured the deuterium contamination in commercial ^{3}He gas by detecting HD^+ separately via Accelerator Mass Spectrometry. The experiment was carried out using the RCNP K=140 AVF cyclotron. The cyclotron accelerator and the NEOMAFIOS ECR (NEOMAFIOS) ion source were operated only for the experiment on the beam injection line at an annex leading to the post accelerator (RCNP Ring cyclotron). The present result is $HD^+/{}^3He=(3.82\pm0.69)\times10^{-5}$. Even if the ECR ion source uses electrons with higher energy than that of a duoplasmatron ion source there is a considerable amount of HD^+ production from the surface of the ion source and from the bottle of ^{3}He gas.

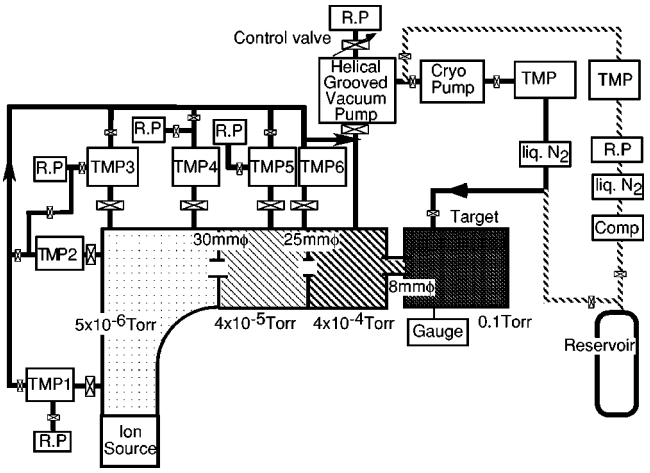

FIG. 3. Complete layout of the windowless gas target evacuation and recirculation system. TMP: Turbomolecular pump. R.P: Rotary pump.

Deuteron contamination in the target was also estimated during operation of the recirculation and purification system. The pressure was 1.2×10^{-2} Torr at the target and 7.6×10^{-7} Torr at the helical grooved vacuum pump. The H_2O component in the residual gas was measured by means of a quadrupole mass spectrometer, to be about 20%. Assuming that the amount of H_2O at the target gas is the same as the residual gas, and the deuteron abundance is the same as the natural abundance (0.014%), we can deduce that the deuteron contamination (D_2O) is in the order of ppm. This is satisfactory for the present measurement as will be discussed later. In addition, the amount of deuterium contamination in the target gas was also evaluated by means of the ^{3}He+^{3}He experiment, by detecting the 14.7 MeV proton, and was found to be about 0.1 ppm.

D. Calorimeter

A calorimetric device has been developed to measure the projectile flux in the present experiment, since the charge integrating method is not applicable due to the neutralization of the incident charged particles with the gaseous target.

Many types of calorimeters have been developed [8]. There are two types of calorimeters. One type measures the temperature difference between two parts thermally isolated with large heat resistance material. The other type measures the power needed to stabilize the temperature of water used to cool the calorimeter cup which is bombarded with energetic particles.

We developed a calorimeter by using a heat flux sensor with an accuracy of better than 5% in the dynamical range of 1–30 W [9].

The structure of our calorimeter is shown in Fig. 4. It consists of a solid copper heat sink (100 mm length, 38 mm diameter) with water channels, and a Faraday cup (140 mm length, 38 mm diameter, 1.5 mm wall thickness) in front of the heat sink. The Faraday cup is supported by a Pyrex glass insulator as well as a metal flange with a Teflon gasket. This organic gasket served as a vacuum seal as well as an electric

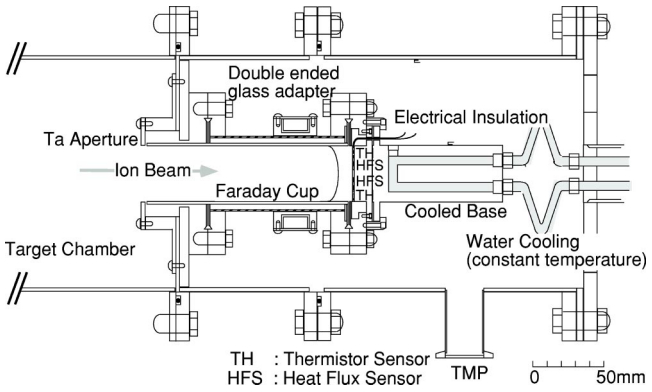

FIG. 4. Cross sectional view of the calorimeter.

insulator. Therefore, this calorimeter can also measure the number of incident particles, when the target chamber is in vacuum, by an electrical current. At the entrance of the cup, a secondary electron suppressor is installed. Around 100 Vwas applied to the suppressor for the current measurement.

After passing through the windowless gas target, the incident $^3He^{1+}$ and $^3He^{2+}$ beam is neutralized and captured in a Faraday cup and calorimeter. In order to be applicable to a wide current range, a heat flux sensor (HFS) (OMEGA HFS-3) was used to measure the heat transfer from the hot part to the cold part. The HFS is a thermistor bolometer which can measure the heat flux to or from a surface with minimum disturbance of the existing heat flow. In this method, a self-generating thermopile is arranged around a thin thermal barrier to produce a voltage that is a function of the thermal energy passing through the sensor. The response of the sensor to the thermal energy input is 1.10–1.11 mV/W/m^2. For a precise measurement of the heat transfer, we made use of the following procedures: (1) In vacuum, the current of the ion beam can be measured by standard charge integration where the calorimeter cup serves as a Faraday cup; (2) to reduce the conduction and convection losses, the heat capacity of the calorimeter should be reduced by as much as possible in order to get a better time response. With the present heat flux sensor, temperature differences of less than 0.001 °C can be detected easily. Therefore, the temperature of the heat sink of the calorimeter should be stabilized to better than 0.1 °C with heat exchange. As shown in Fig. 4, between the copper base and the thin plate of the calorimeter, two heat flux sensors are sandwiched with thermistor temperature sensors. These are originally insulated electrically. As shown in Fig. 4, thermistor temperature sensors are also located to measure the temperature of the ambient or Faraday cup base and the cooled heat sink. These are installed in a stainless steel pipe (40 mm length, 10.5 cm diameter), which can be evacuated by a small turbomolecular pump.

The calorimeter was tested by using a $^3He^{2+}$ beam of energy of 40 kV (80 keV). The relation between beam current (I) and heat flux (H) can be written as

$$I\,\delta t = k_1 H\,\delta t + C\,\delta T, \tag{1}$$

where T is the temperature of the calorimeter and C is the heat capacitance. The term $C\delta T$ shows that the temperature of the calorimeter depends on the incident beam current. Thus, if the intensity I is changed, the converted heat is used to heat the calorimeter and is also transferred to the cold base.

Since the transferred heat may be approximated to be proportional to the temperature difference between the front and cold base, the second term in Eq. (1), $C\delta T$, can be rewritten as $k_2\delta H$. Thus, Eq. (1) can be written as

$$I = k_1 H + k_2 \frac{\delta H}{\delta t}. \tag{2}$$

In order to determine the parameters k_1 and k_2, an experiment was carried out with a $^3He^{2+}$ beam of 40 keV ($E_{c.m.}$). The beam current was calculated from the HFS output by comparison with the Faraday cup measurements. The HFS output was measured by a KEITHLEY 2000 multimeter. The parameters k_1 and k_2 were determined as follows.

(1) Parameter k_1: If the system is stable, that is, incident beam I and temperature T are stable, the second term of Eq. (2) can be ignored. In this condition, the parameter k_1 can be determined by a least squares fit as shown in Fig. 5(a).

(2) Parameter k_2: This parameter can be determined once parameter k_1 is known, as seen in Eq. (2). The term $\delta H/\delta t$ was measured for averaged time scales of 3, 7, 15, and 30 sec. It was found that the scale of 30 sec was appropriate. Figure 5(b) shows $\delta H/\delta t$ as a function of $(I-k_1)H$.

(3) Comparison with beam current: Fig. 6 shows the beam current as a function of time measured using a Faraday cup, k_1H, and $k_1H+k_2(dT/dt)$ with different beam conditions, i.e., stable, slowly increasing, and decreasing beam current.

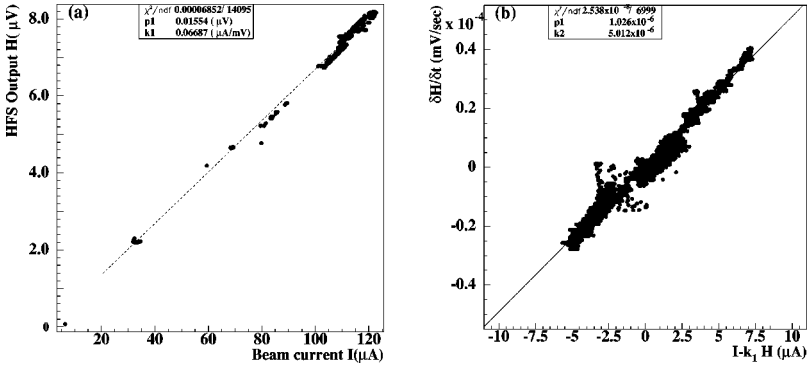

FIG. 5. (a) Measured beam current [$I(\mu A)$] vs heat flux [H(mV)], under the condition of $\delta H/\delta t = 0$ in Eq. (2). The parameter k_1 in Eq. (2) is derived by fitting with a linear function. (b) Plot of $\delta H/\delta t$ [Eq. (2) in text] as the difference of $(I - k_1)H$. The parameter k_2 in Eq. (2) is derived by fitting with a linear function.

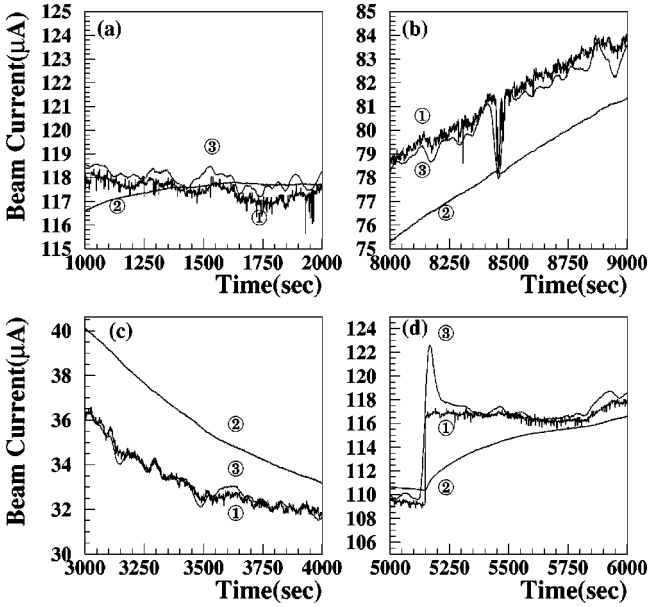

FIG. 6. Beam current, ① measured by the Faraday cup, ② calculated from k_1H, and ③ $k_1H+k_2(\delta H/\delta t)$ as a function of time. The measurements were carried out for (a) stable beam current, (b) increasing beam current, (c) decreasing beam current, and (d) for rapid beam step of current.

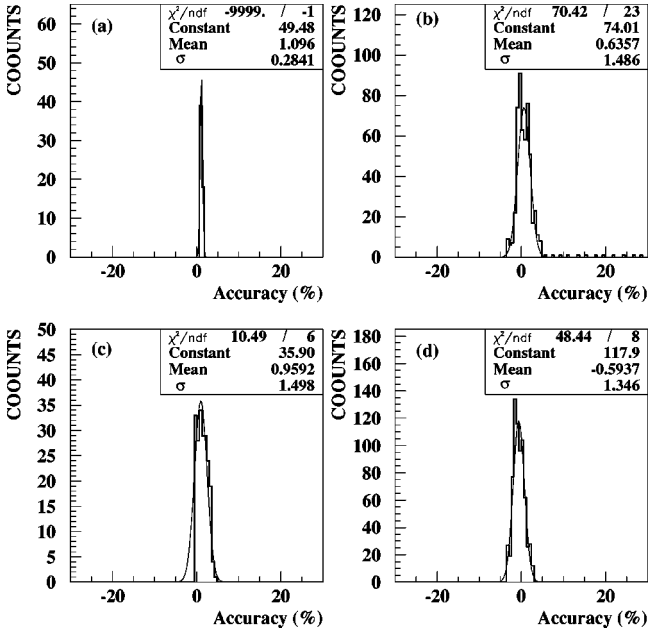

FIG. 7. The accuracy of the beam current for different beam energies (a) 35, (b) 30, (c) 25, and (d) 20 keV, in the form of (IHFS-IFC)/IFC, where IHFS and IFC denote the beam currents measured by the HFS and the Faraday cup (FC).

The calculated currents measured with the HFS reproduce the measurements with the Faraday cup as shown in Figs. 6(a)–6(c). On the other hand, if the beam current is suddenly changed as shown in Fig. 6(d), the calculated currents from the HFS output overestimate the value measured by the HFS. Further improvements of this system are necessary. Fortunately, this should not be a fatal problem for an astrophysical experiment with a long term measurement duration of typically 1 day or 1 month, since this occurs rarely, at most one or two times in a day. Thus, in the experiment, the error caused by this overestimate can be neglected.

1. Reproducibility of beam current for different energies

The reproducibility of the beam current determined from the HFS output was verified for several beam energies. Measurements were carried out on $^3He^{2+}$ beam at incident kinetic energies of 35, 30, 25, and 20 keV. The beam currents were calibrated using the parameters determined with the 40 keV beam. Figure 7 shows the accuracy of the calculated beam current in the form of $(I_{HFS}-I_{FC})/I_{FC}$, where I_{HFS} and I_{FC} are the beam currents measured by the HFS and the Faraday cup (FC), respectively. The accuracy was better than 2% for the measured energies.

2. Estimation for transferred heat in HFS

The heat transferred through HFS can be calculated from the calibration parameter of HFS (OMEGA HFS3: 1.10–1.11 μV/W/m^2 at 70°F).

3. Heat exchange with the surroundings

Because of the different vacuum conditions during the calibration ($\sim 10^{-6}$ Torr) and during the experiment (0.1 Torr), the effects of convection heat losses by the gas flowing in the target chamber have to be estimated. The heat transmission by convection was measured by comparing the transferred heat through the HFS for the two conditions of vacuum (10^{-6} Torr and 0.1 Torr) in the target chamber. The temperature of cool base was 30°C. The difference of HFS output was 0.04 W corresponding to about 1.7% for a 35 keV 100 μA beam.

E. $dE-E$ counter telescope

In order to ensure a large detection efficiency and a clear discrimination of real events, we exploit four $dE-E$ counter telescopes by using semiconductor detectors for the measurement of the ^{3}He(^{3}He, $2p$)^{4}He reaction. These detectors are installed into the target chamber filled with ^{3}He gas and are capable of identifying the ^{3}He+^{3}He reaction (Q =12.86 MeV) as shown in Fig. 8.

The reaction generates two protons which have kinetic energies of 0–10.7 MeV, and an α particle which has kinetic energies of 0–4.3 MeV. The dE and E detectors in each telescope have an active area 2500 mm^2, the dE detector has a thickness of 140 μm, and the E detector has a thickness of 1500 μm (MICRON Ltd.).

To stop the generated α photons, and elastically scattered ^{3}He from the beam, aluminized Mylar films with thickness of 25 μm are located in front of all dE counters. The distance between the dE counter or E counter and the beam axis is 32.5 mm and 37.1 mm, respectively. These detectors are fixed to a base of oxygen-free high conductive copper. It is helpful to avoid microphonic noise and natural background.

F. Data acquisition system

Analog signals from each detector are fed into preamplifiers (model 142IH, ORTEC, for dE counters model 142B,

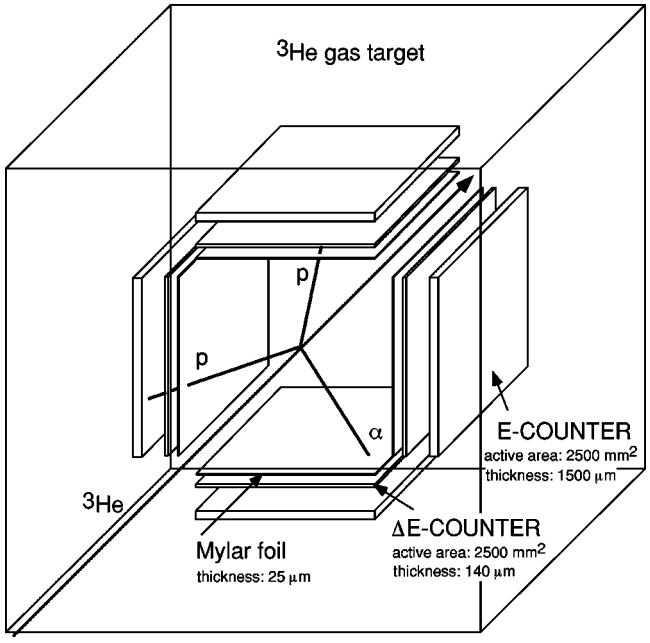

FIG. 8. Schematic view of detector assembly.

ORTEC, for *E* counter) with inorganic coaxial cables (Cu-S5ESS-05 DIPSOL CHEMICAL Co.,Ltd.). Since a shorter distance between the detector and preamplifier is desirable to reduce electrical noise, the distance is 45 cm. The signals from the preamplifiers are amplified by both spectroscopy amplifiers (SAMP, model 472 ORTEC) and timing filter amplifiers (TFA, model 454, ORTEC). The signals from the SAMP are led to a CAMAC peak sensitive analog-digital-converter system (ADC, model AD811, ORTEC) while the signal from the TFA's are sent to a system of constant fraction discriminators (CFD, model 935, ORTEC) where the thresholds are set above the noise level of the detectors. The logic output of the CFD is fed into a logic Fan-In/Fan-Out (Fan-I/O, model 429A, ORTEC) delivering a gate signal for the CAMAC ADC's with a gate width of 400 nsec. The logic output provides a start signal for a time spectrum via a CAMAC time-digital-converter system (TDC, model 2228A, Lecroy). The stop signal of the TDC's is provided by the CFD with a 100 nsec delay. The signals from the ADC and TDC systems are controlled by a CAMAC crate controller (model CC7700, TOYO). The data from the crate controller are transferred to Linux station (model L400c, DELL), via a CAMAC bus, and stored on hard disk. A schematic diagram of the present data acquisition system is shown in Fig. 9.

The dead time of this data taking system is 400 μsec for one event. The typical counting rate of the measurement of the ^{3}He+^{3}He reaction, which includes the background events caused by ^{3}He+d reaction, cosmic ray, and electrical noise is usually about 3 counts/sec. Therefore, the total dead time of these measurements is about 0.1%.

Before the reaction experiments, all the counters were calibrated using a ^{241}Am α source (5.48 MeV). The energy resolution of the *dE* counters was 100–120 keV [full width at half maximum (FWHM)] for a 5.48 MeV α particle, and for the *E* counter it was 70–100 keV (FWHM). The energy gain of SAMP was optimized to be able to measure the energy range up to 10 MeV for the *dE* counter and 20 MeV for the *E* counter. This energy range is required to measure not only ^{3}He+^{3}He events but also ^{3}He+d events, since ^{3}He+d events are needed for estimation of the background and are useful for checking the energy scale of each counter telescope. The linearity of the present amplifier system was measured by use of a precision pulse generator (model 419, ORTEC). Linearity was observed to within 0.05% for all of the energy range of each counter. The stability of the energy gain of the amplifiers was checked and the resultant gain shifts were less than 2% for 6 months.

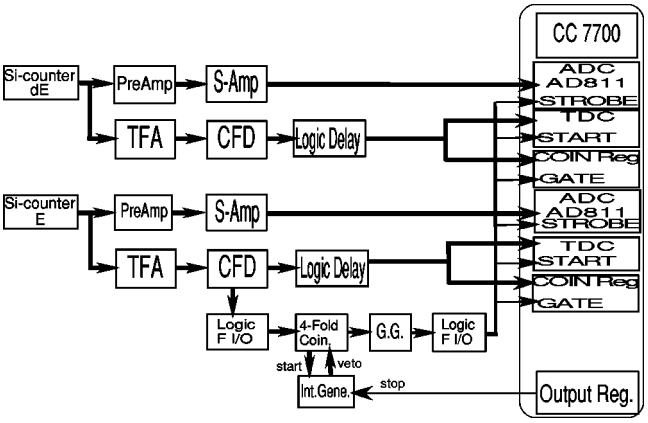

FIG. 9. View of electronics for data acquisition.

III. ANALYSIS OF EXPERIMENTS

For evaluation of the cross section, the number of counts for the ^{3}He(^{3}He, 2p)^{4}He reaction, the ^{3}He target density, and the ^{3}He beam intensity should be measured. The values for the effective reaction energy and the integral term for detection efficiency were calculated by means of a Monte Carlo simulation developed for the present work.

The number of counts $dN(z)$ per unit of time with respect to a length dz of the extended ^{3}He gas target is given by the expression

$$dN(z) = N_t N_b \sigma(E(z))\,\eta(z) dz, \tag{3}$$

where $N(z)$ is the number of counts for the ^{3}He(^{3}He, 2p)^{4}He reaction, N_t is the ^{3}He target density, N_b is the ^{3}He beam intensity per unit time, and $\eta(z)$ is the absolute detection efficiency.

Introducing the stopping power ϵ (i.e., the energy loss per unit length), Eq. (3) can be rewritten in the form

$$dN(E) = N_t N_b \sigma(E)\,\eta(E)\,\epsilon(E)^{-1} dE. \tag{4}$$

The total number of counts for the full target length is then given by

$$N = N_t N_b \int_L \sigma(E)\,\eta(E)\,\epsilon(E)^{-1} dE. \tag{5}$$

For the case of a thin target, introducing an effective reaction energy E_{eff} corresponding to the mean value of the projectile energy distribution in the detection setup, one arrives at

$$N = N_t N_b \sigma(E_{\text{eff}}) \int_L \eta(E) \epsilon(E)^{-1} dE. \quad (6)$$

A. Effective reaction energy

The effective reaction energy was the mean value of the beam energy derived from an energy loss calculation in the target gas. As we could not make any measurement for the absolute energy of ion beam, such as a time of flight technique or an Wien filter, we determined the value by measuring a voltage divided with a precise register chain of a ratio of 1/10 000 (STANDARD ENERGY, S-100) for the applied voltage to the ion source [SPELLMAN, SL-1200 (60 kV/20 mA)]. This resistive voltage divider was investigated by applying the exact voltage calibrated with the second standard, and the resultant absolute accuracy is ±0.2%. It was measured at intervals of 1.5 sec for all measurements. The stability of the voltage was less than 0.1% for about 1 day.

Compared with an ion source of a quiescent plasma, such as a duoplasmatron ion source, an ECR ion source has a finite plasma potential. Thus, we took into account this plasma potential for the acceleration voltage. The adopted value was 21.3±2.4 eV as reported in Ref. [10] by Saito *et al.*, for the NANOGUN ECR ion source.

For the extended geometry in the present gas target experiment, the reaction energy distribution due to the energy loss of the ion beam along the beam path should be estimated as precisely as possible. In low-energy experiments, this might raise the ambiguity for the electron screening potential; we had to take care of experimental conditions such as target pressure or its difference along the beam axis. In this series of experiments for energies less than 30 keV center of mass energy, the problem should be treated more rigorously.

There are quite number of experimental and theoretical papers on stopping powers of charged particles in matter. Charged particles lose their energy through collisions with nuclei and with atomic electrons in matter. Although the greatest part of the energy loss occurs by collisions with electrons, low-energy ions lose their energy by collisions not only with electrons but with nuclei. Since it is impossible to deduce the stopping power data near the zero energy, using present-day technology, we have used updated compilations with an accuracy of ranges between 2% and 10% [11]. Therefore to calculate the energy loss in the target, we used the stopping power values estimated by the SRIM computer code [12], which gives results consistent with the experimental energy losses to within a 10% difference at most.

For example, the stopping power of incident ^{3}He with an energy of E_{lab}=90.00 keV is 9.3×10^{-15} eV/atom/cm^2. The energy distribution of this particle in the ^{3}He gas target with a pressure of 0.1 Torr is simulated by our Monte Carlo program and the result is shown in Fig. 10.

We employ the full target length of L=30 cm as the distance between the entrance of the target just after the collimator and the entrance of the beam calorimeter. Since the rapid reduction of the cross section is about 11.2% at $E_{\text{lab}}(^3\text{He})$=90 keV over the target thickness when we assumed a constant $S(E)$ factor, the effective energy loss is evaluated to be (500±50) eV. This value roughly agrees with the estimated value of 493 eV for the energy loss between the entrance and the center of the counter telescope on the beam axis. As shown in Fig. 10, we simulated the effective target length and estimated energy spread of 79 eV as the error of the incident beam energy. The energy loss due to the residual gas between the ion source and the target entrance is (3.7×10^{-3})% of the incident beam energy.

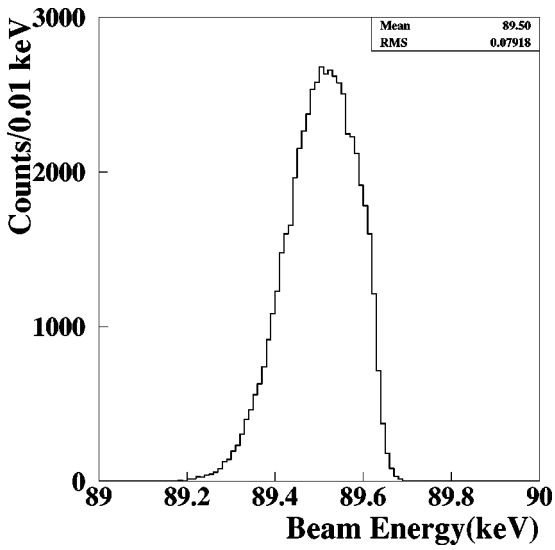

FIG. 10. Simulated interaction energy distribution for ^{3}He + ^{3}He reaction at E_{lab}=90.0 keV. A target gas pressure of 0.1 Torr is assumed.

In summary, at an incident beam energy of (90.0±0.13)keV, the effective reaction energy is E_{lab} =(89.50±0.13)keV, thus a 0.15% accuracy for the reaction energy, taking into account the accuracy of 0.1% for the acceleration voltage, 10% for the stopping power, and 0.09% for the energy spread in the target.

B. Beam current

The incident projectile number (N_b) is deduced from the deposited power measured with our calorimetric device as described in the preceding section. It was calibrated using a charged beam in vacuum by comparing with the electrical beam current in the Faraday cup. The electrical charge collected in the Faraday cup was measured with the current integrator (KEYTHLEY 616 digital electrometer). The absolute value of the current integrator was calibrated by measuring the current which was supplied with a precise current source (R6161 ADVANTEST). It has an accuracy and a stability better than 0.001%. The difference between the current measured by the current integrator and the value of the current source is less than 3% and it was corrected. The following was taken into account to evaluate the incident particle number N_b. The beam current measured by the calorimeter was corrected because of the energy loss of the incident beam in the target gas. The energy loss was estimated by the SRIM program and was 1.60±0.16 keV when the incident

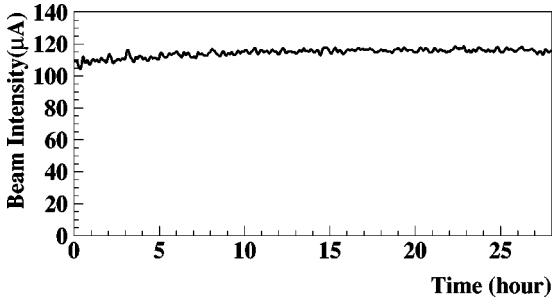

FIG. 11. Measured intensity of $^3He^{2+}$ beam at $E_{lab}=90.0$ keV. Measurements were made at 1.5 sec intervals.

beam energy was 90.0 keV ($E_{c.m.}=45.0$ keV). This energy loss was 1.8% lower than the incident energy.

The intensity was simultaneously corrected by recording the beam energy and the target gas pressure at intervals of 1.5 sec. The typical beam intensity was about 100 μA at an incident energy of 90 keV for the $^3He^{2+}$ beam. The beam intensity measured by the present system during experiment is shown in Fig. 11.

C. Target density

There are several factors which affect the target density N_t such as the gas temperature and a pressure gradient in the target chamber. We measured the target gas temperature with a thermistor (103AT-2) inside the chamber which was likely to be different from that of the laboratory room since the target gas was heated by the beam and cooled by the circulated gas for the purification system.

As the target pressure could not be measured directly at the beam-target interaction region during the experiment, the pressure was measured at the top of the target chamber as shown in Fig. 12. The pressure distribution caused by the geometry of the detector holder, collimators, and gas circulation was measured by extending the stainless tube directly from the capacitance manometer set downstream of the target chamber before the experiment. The capacitance manometer, which is usually installed at the top of the target chamber, was removed to the end of the chamber only at this measurement, as shown in Fig. 12. Simultaneously, we used another gauge just before the inlet to the chamber for a normalization. The difference between the target gas pressure at the top of the chamber and that measured at the interaction region was rather small, which might be a shorter mean free path at a gas pressure of the order of 0.1 Torr. The absolute pressure at the target should be corrected by 5% less than that measured at the top of the chamber. Owing to these corrections, the target density can be determined to an accuracy of 1.3%, considering the accuracy of 0.16% from the target gas pressure, 1% from the correction due to the gas temperature, and 0.8% from the correction due to the measurement position. The measured target gas pressure at the every interval of 1.5 sec is shown in Fig. 13.

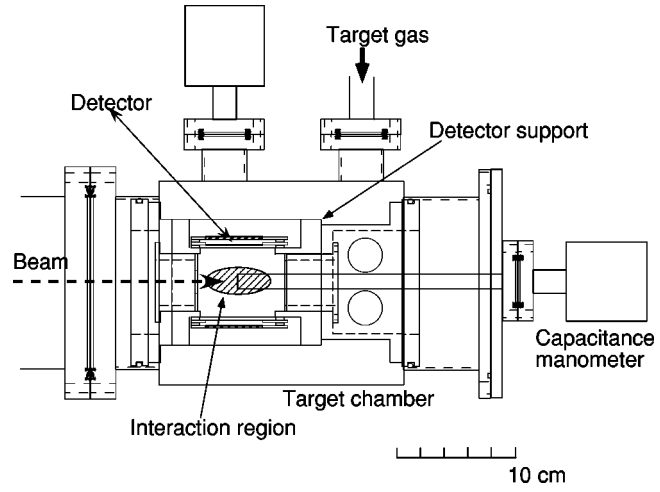

FIG. 12. Schematic view of the measurement of the gas pressure at the interaction region between the beam and gas target.

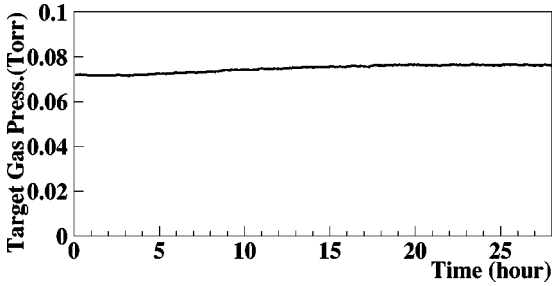

FIG. 13. Measured target ^3He gas pressure by Baratron capacitance manometer. Measurement intervals were 1.5 sec for all experiments for the $^3He+^3He$ reaction. The pressure was normalized to that of temperature at 0 °C.

IV. DATA ANALYSIS

A. Monte Carlo simulation for the OCEAN experiment

In order to find an optimum detector setup for a high efficiency and background-free measurement, we exploit the Monte Carlo simulation program based on GEANT3. It was used to calculate the interaction between the ejectiles and the detectors. Also, the GENBOD code was used to generate the ejectiles. Thus the program takes into account the following aspects: (1) the detector geometry, (2) the energy loss and energy straggling of the ejectiles in both the target gas and the thin foil in front of the detector, (3) kinematic effects on the energy of the ejectiles in the target, (4) yield dependence of the ejectiles over the passage of the target, and (5) the nonuniform depletion thickness for the *E* counter.

B. Measurement of the D(^{3}He, *p*)^{4}He reaction

To verify the validity of the simulation program, that is, to estimate the systematic error in detection efficiency, the experimental results of the D(^{3}He,*p*)^{4}He reaction ($Q=18.4$ MeV) are compared with those of simulations. The comparison to this reaction has several advantages: (1) The generated protons from the ^3He+d reaction have a definite energy of 14.7 MeV; (2) the energy of the protons from this reaction is almost the same as that from the $^3He+^3He$ reac-

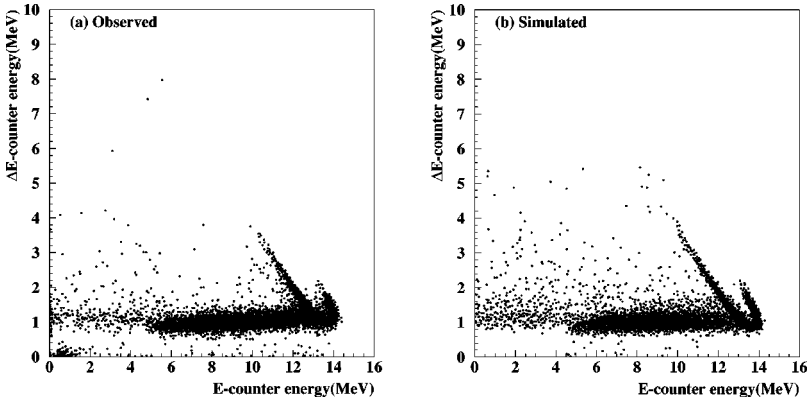

FIG. 14. The (a) observed and (b) simulated energy spectrum for the $d(^3\mathrm{He}, p)^4\mathrm{He}$ reaction at $E_{^3\mathrm{He}}=90.0$ keV by means of the $dE-E$ counter telescope.

tion; (3) the cross section of the $^3\mathrm{He}+d$ reaction is six orders of magnitude larger than that of $^3\mathrm{He}+^3\mathrm{He}$ reaction.

The $\mathrm{D}(^3\mathrm{He},p)^4\mathrm{He}$ reaction was performed by using 90 keV ($E_{\mathrm{c.m.}}=45$ keV)$^3\mathrm{He}^{2+}$ beam at the OCEAN facility. The target pressure of the deuterium gas was maintained around 10×10^{-4} Torr.

Figure 14 shows observed and simulated energy spectra obtained with the $dE-E$. The broad energy spectra for $E=5-14$ MeV at $dE=1$ MeV arise from an insufficient depletion depth for protons incident on the surface at angle near 90°. We applied a bias voltage of 180 V to the E counter, which corresponds to the depletion depth of 900 μm, to avoid a discharge in the gas target (thicker depth needs more voltage). The other two structures arise from kinematics effects in combination with protons which are incident at angular ranges of 135°–180° and 0°–45°. These three remarkable features are well simulated in the energy spectrum as shown in Fig. 14(b).

C. Background analysis

It is crucial for the present measurement of the $^3\mathrm{He}(^3\mathrm{He}, 2p)^4\mathrm{He}$ reaction to identify the background origin and to discriminate the true events from the fake events. As already stated, deuterium contamination in the target is the most serious. The number of deuterons in the gas target was determined from the data during the measurement of the $^3\mathrm{He}(^3\mathrm{He}, 2p)^4\mathrm{He}$ reaction as shown in Fig. 15. For this estimate, the value of the cross section for the $\mathrm{D}(^3\mathrm{He}, p)^4\mathrm{He}$ reaction was taken from Ref. [13]. We conclude that the deuterium contamination is 0.2 ppm in the target gas, and that such a level could make background events of only 0.1% of the observed events of the $^3\mathrm{He}(^3\mathrm{He}, 2p)^4\mathrm{He}$ reaction at the energy of $E_{\mathrm{c.m.}}=45$ keV.

Another source of background events arises from electrical noise and cosmic rays. These are observed during the measurement without the ^{3}He beam for 38 days of operation of OCEAN as shown in Fig. 16. The contribution from this background to the window of the $^3\mathrm{He}(^3\mathrm{He}, 2p)^4\mathrm{He}$ reaction is 3.6 counts/day. Of these, the cosmic muon events are located around $dE=70$ keV and $E=450$ keV because of the minimum ionization loss of 2 MeV cm^2/g. We attempted to reject these events by applying the vetocounter upper and lower places for the target chamber. Finally the expected rate of the present reaction at the lower energy is around a few events per day or less, and a typical single background rate of silicon detectors is one event per hour or more. In order to remove such accidental events, two-proton coincidence should inevitably be required for the identification of the present reaction near the Gamow peak (next series of OCEAN experiment).

D. Detector efficiency

We developed a reasonable method to determine the acceptable area for the real events of the $^3\mathrm{He}(^3\mathrm{He}, 2p)^4\mathrm{He}$ reaction in the $dE-E$ scatter plot without a redundant and ambiguous procedure. Four types of data such as observed events of the reaction, simulated events for the $^3\mathrm{He}(^3\mathrm{He}, 2p)^4\mathrm{He}$ reaction and for the $\mathrm{D}(^3\mathrm{He},p)^4\mathrm{He}$ reaction, and observed background events are summarized for the analysis of each experimental run. The energy distribution of the $dE-E$ scatter plot is divided into 16 000 parts of 100 keV$\times$100 keV parts as shown in Fig. 17. The signal to

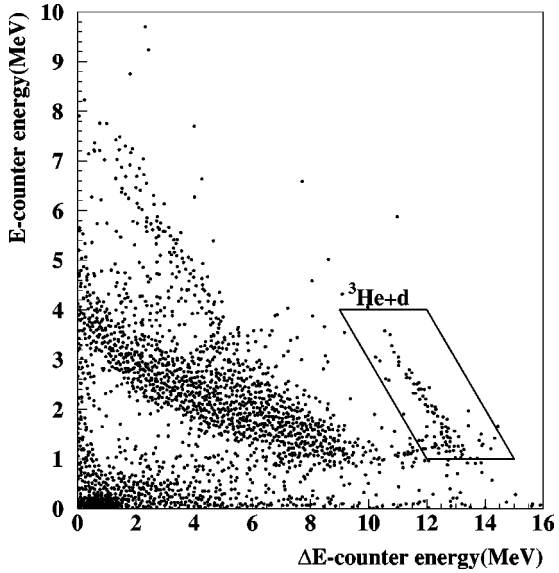

FIG. 15. Observed $dE-E$ energy spectrum of the $^3\mathrm{He}(^3\mathrm{He}, 2p)^4\mathrm{He}$ and $\mathrm{D}(^3\mathrm{He}, p)^4\mathrm{He}$ reactions. The solid line shows the acceptable energy region for the $\mathrm{D}(^3\mathrm{He}, p)^4\mathrm{He}$ reaction. The deuteron contamination in the target ^{3}He gas was evaluated from the events in this region.

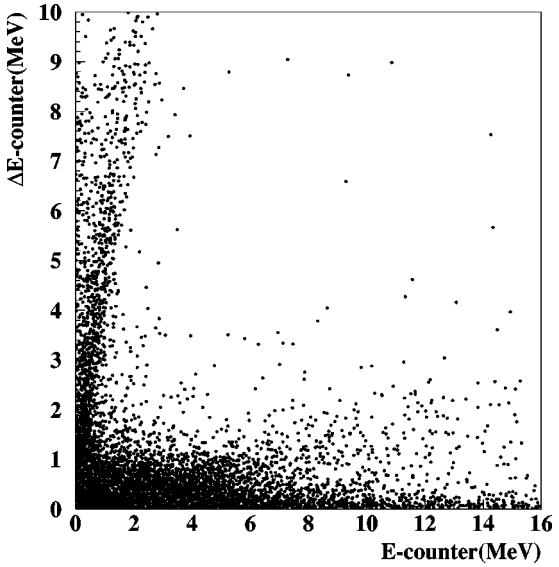

FIG. 16. Background events arising from electronic noise and cosmic ray, observed with the same geometry as the ^{3}He(^{3}He, 2p)^{4}He experiment.

noise (S/N) ratio, which can be derived from the Monte Carlo (MC) (^{3}He+^{3}He) divided by MC(^{3}He+D) and measured background, was allotted for 16 000 parts. All parts are ordered as a function of their S/N ratio; parts having a better S/N ratio are located at the right-hand side while worse parts are located to the left, as shown in Fig. 18. Figure 18(a) shows the distribution of the simulated events from the ^{3}He+^{3}He reaction as a function of S/N ratio. Many events are located on the right-hand side in the figure, which should correspond to the better S/N ratio. Also, Figs. 18(b) and 18(c) show the distribution of the simulated events for ^{3}He $+d$ reaction events and the observed background events as

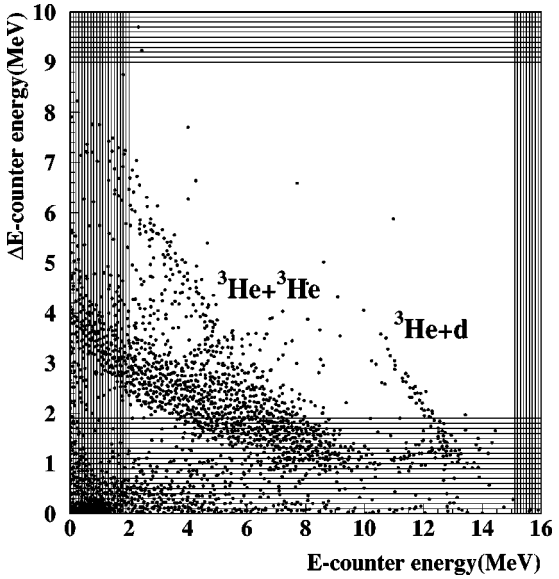

FIG. 17. Schematic view of the the acceptance region. The $dE-E$ energy scatter region was divided into 16 000 parts of 100 keV$\times$100 keV divisions. Signal to noise ratio was examined in each part.

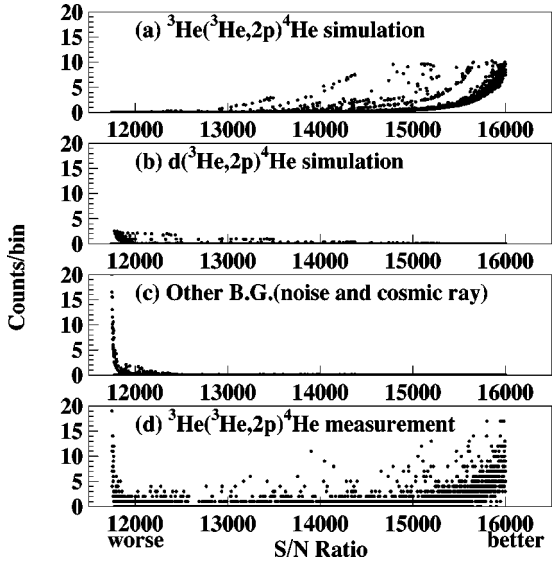

FIG. 18. Event distribution ordered as a function of their S/N ratios for four types of data. The parts having a better S/N ratio locate at the right-hand side while worse parts are located to the left. (a) simulated ^{3}He+^{3}He, (b) simulated ^{3}He+d, (c) other observed background (electric noise and cosmic ray), (d) observed ^{3}He+^{3}He are shown. S/N ratio is given by S (simulated ^{3}He+^{3}He)/N(simulated ^{3}He+d+observed other background).

discussed above. It is usual that these background events should be located on the left-hand side of each figure. Figure 18(d) shows the distribution of the observed event for ^{3}He $+^3$He reaction at $E_{\mathrm{c.m.}}$=45 keV, as a function of S/N ratio. The contribution from the background events is apparently very small. Therefore the observed distribution as shown in Fig. 18(d) is very similar to the simulated one, shown in Fig. 18(a), without subtraction of any background events as shown in Fig. 18(d).

Since, most of the background events exist at less than 13 000 in allotted number for each part (Fig. 18), the acceptable area for the ^{3}He+^{3}He reaction could be assigned to channels larger than 13 000 channel. The region of that is shown in Fig. 19.

Experimental results are as follows: 3344 counts are observed in the acceptable region, while the contribution from the ^{3}He+D events to the region is 20.9 counts, and that from the other background component is 2.46 counts. After subtracting the number of these background events from the number of observed events in the acceptable region, the number of true events for the ^{3}He+^{3}He reaction is 3337.4, with a statistical error of 1.8%. According to this procedure, the detection efficiency $\eta(x)$ can be written as

$$\eta(x) = \sum_{i=x}^{16\,000} N_a(i), \tag{7}$$

where $i=x$ to 16 000, $N_a(i)$ is the number of counts for the simulated distribution, and x is the parameter of the boundary cut point for the accepted events. The accepted events have been derived as

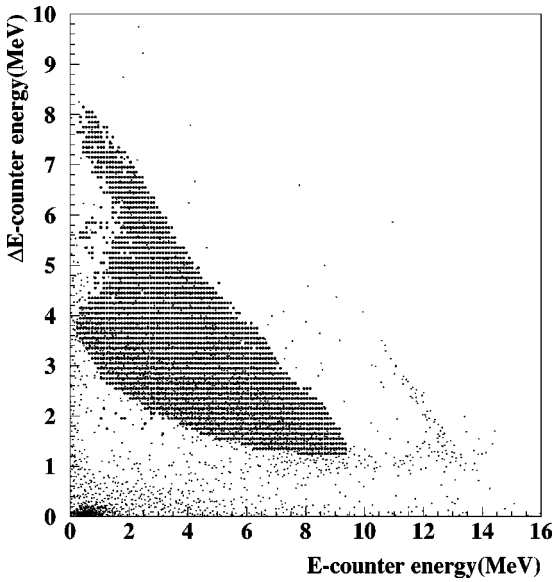

FIG. 19. $dE-E$ scatter plot obtained from the ^{3}He+^{3}He reaction experiment. The region assembly of heavy solid points shows the accepted region as the true events from the ^{3}He(^{3}He, $2p$)^{4}He reaction.

$$A(x) = \sum_{i=x}^{16\,000} \{N_d(i) - N_b(i) - N_c(i)\}, \tag{8}$$

where $A(x)$ refers to accepted events for the ^{3}He(^{3}He, $2p$)^{4}He reaction, $N_d(i)$, $N_b(i)$, $N_c(i)$ are the number of counts for the observed events, for the D(^{3}He, p)^{4}He, and for other background events, respectively. Finally the ratio of $A(x)/y(x)$ corresponding to the cross section of the ^{3}He(^{3}He, $2p$)^{4}He reaction can be obtained. The ratio slightly depends on the boundary parameter x as shown in Fig. 20. Thus, the accuracy of the simulated energy distribution in a scatter plot should be derived from the fluctuation of this ratio. When we include the geometrical uncertainty of the counter telescope, i.e., 0.5% uncertainty of the detection efficiency simulated with the Monte Carlo program, the systematic error of the detection efficiency is evaluated to be 3%.

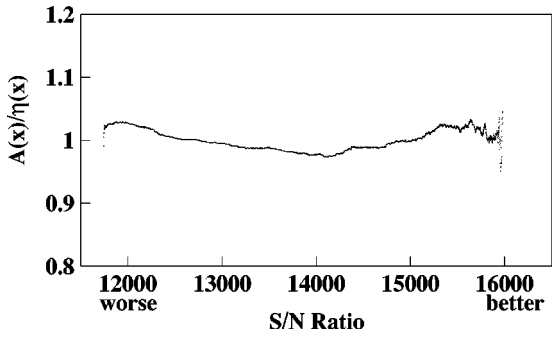

FIG. 20. Ratio of $A(x)/\eta(x)$ as the function of the boundary parameter x. The ratio corresponds to the cross section of the ^{3}He $+^3$He reaction. $\eta(x)$ and $A(x)$ were derived from Eqs. (7) and (8) (see text), respectively.

V. EXPERIMENTAL RESULTS AND DISCUSSION

The experimental results for the cross section and S factors obtained for the first series of OCEAN experiments from the year 2000, together with the experimental conditions such as the live time, beam current, the target gas pressure, and the target temperature are shown in Table II. The observed events for the ^{3}He(^{3}He, $2p$)^{4}He reaction and the background events from various sources are also shown in Table II. In Table III, from the accuracy of each term due to beam intensity, reaction energy, target density, and detector efficiency, a sum of the systematic errors is estimated to be 3.8%.

The cross section for the ^{3}He(^{3}He, $2p$)^{4}He reaction has been derived from the following equation,

$$N = N_t N_b \sigma(E_{\text{eff}}) \int_L \eta(E)\epsilon(E)^{-1} dE, \tag{9}$$

where N is the number of counts for ^{3}He(^{3}He, $2p$)^{4}He reaction, N_t is the ^{3}He target density, N_b is the ^{3}He beam intensity, E_{eff} is the effective reaction energy, $\eta(E)$ is the

TABLE II. Summary of measurements for the ^{3}He(^{3}He, $2p$)^{4}He reaction. L.T., live time; BC, beam current; TP, target pressure; TT, target temperature; CS, cross section; True, ^{3}He+^{3}He; BG1, BG ^{3}He+d; BG2, BG other; Cnt, counts; S-fac, astrophysical S factor with statistical error. The sum of the systematic errors in S factor is 3.8%.

$E_{\text{c.m.}}$ (keV)	LT (sec)	BC (μA)	TP (Torr)	TT (°C)	True (Cnt)	BG1 (Cnt)	BG2 (Cnt)	CS (barn)	S-fac (MeV b)
45.3	92567	104.	7.46×10^{-2}	27.1	3276	20.9	2.46	1.53×10^{-8}	5.39 ± 0.09
43.3	78647	91.4	6.72×10^{-2}	27.3	1374	7.50	2.09	9.55×10^{-9}	5.43 ± 0.14
41.3	80687	100.	6.74×10^{-2}	27.1	939	7.08	2.15	5.79×10^{-9}	5.51 ± 0.18
39.3	83109	87.4	7.26×10^{-2}	27.0	542	6.08	2.21	3.44×10^{-9}	5.69 ± 0.25
37.3	155442	112.	8.24×10^{-2}	29.3	770	17.0	4.14	1.83×10^{-9}	5.46 ± 0.20
35.2	338862	100.	8.21×10^{-2}	29.3	770	21.4	9.02	9.46×10^{-10}	5.62 ± 0.21
33.1	615814	103.	8.25×10^{-2}	30.4	691	11.4	16.4	4.52×10^{-10}	5.48 ± 0.22
31.2	528134	93.6	8.28×10^{-2}	30.3	293	5.02	14.1	2.46×10^{-10}	6.40 ± 0.39

TABLE III. Estimated systematic error due to beam intensity, reaction energy, target density, and detector efficiency, for present experiment together with existing data by Krauss *et al.* [3] and LUNA [2].

	Reaction energy (%)	Beam intensity (%)	Target density (%)	Detection efficiency (%)
Present experiment	0.15	2	1.3	3
Krauss *et al.*	0.27	3	2	4
LUNA	0.09	3	1	2

absolute detection efficiency, and $\epsilon(E)$ is the stopping power.

The astrophysical S factors were deduced from the equation

$$\sigma(E) = \frac{S(E)}{E}\exp(-2\pi\eta), \tag{10}$$

where η is the Sommerfeld parameter given by

$$2\pi\eta = 31.29 Z_1 Z_2 \left(\frac{\mu}{E}\right)^{1/2}, \tag{11}$$

where Z_1 and Z_2 are the nuclear charges of the interacting particles in the entrance channel, μ is reduced mass (in units of amu) and E is the center of mass energy (in units of keV).

Figure 21 compares the present result of $S(E)$ between $E_{\text{c.m.}}=45$ keV and 31 keV against the results of existing data [3]. Our present data are in good agreement with those of existing data. The accuracy of both statistical and the systematic uncertaintics of the present measurement is better than that in Ref. [3].

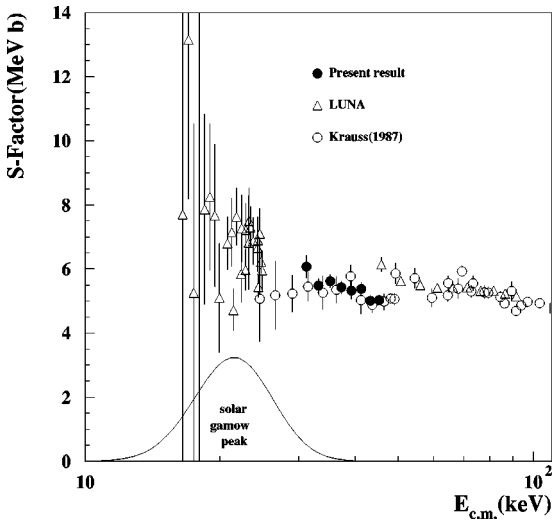

FIG. 21. The S factor of the reaction ^{3}He(^{3}He, $2p$)^{4}He deduced from present measurement (filled circle) and by previous works (circles, Ref. [3]; triangles, Refs. [1,2]). Statistical uncertainties are shown as error bars. Systematical uncertainties on present data (filled circle) are 3.8% (details are given in text), and those on previous works (circles and triangles) are 4%–6% [1–3].

Of the previous studies, experiments between 17.9 and 342.5 kV center of mass energy by Krauss *et al.* cover a wider energy range than others since they used two accelerators of 350 kV accelerator in Munster University and 100 kV facility (DTL) at Bochum University. Recently the LUNA group in the LNGS has presented data down to 16.50 keV center of mass energy. In these previous experiments there was much effort to obtain the scarce true events from the background events, such as deuterium contamination both in the incident beam and in the target gas, cosmic rays (mainly muon) or heavy particles, and electric noise. There have been several solutions for these difficulties; Krauss *et al.* pointed out in 1987 that the purity of the ion beam and of the target were of special interest and they estimated that at 350 keV the mass-3 beam contamination HD^+ was of the order of 10^{-5} [3]. Also they applied proton-proton coincidences to discriminate the real events from intruded events for the D(^{3}He, p)^{4}He reaction, but this might not be applied for the experiment of less than 25 keV center of mass energy. They surrounded the target chamber with a NE102A plastic scintillator in order to identify cosmic events. In this way the unidentified cosmic background coincidence event rate was estimated to be less than one event/200 h in the measurements at $E_{\text{c.m.}}<50$ keV. Another source of background events due to occasional discharges of the accelerator high voltage could be avoided by an amplifier filter or a noise filter. In spite of these efforts, they still find a contribution of the events caused by high-energy protons from the D(^{3}He, p)^{4}He reaction (e.g., 2.5% contribution at $E_{\text{c.m.}}=25$ keV). They also evaluated that the background contribution to the ^{3}He+^{3}He region is 0.40% of the observed counts of the d-^{3}He events.

The measurements at the DTL showed that event rate within the $dE-E$ region of the ^{3}He+^{3}He reaction induced by cosmic rays amounted to 3.5×10^{-4} events/sec, while at LNGS this rate was observed to be reduced by at least a factor 200, that is, 1.8×10^{-6}. It is negligibly small for the low-energy measurement less than 30 keV center of mass energy.

We now argue that the OCEAN facility overcomes these difficulties by applying the following, although there still exists the possibility of background due to the target gas.

(1) Only OCEAN exploits doubly charged ^{3}He ions produced with an ECR ion source and it could avoid the background events due to D(beam)+^{3}He.

(2) The OCEAN facility has been located in an experimental area of the cyclotron and shielded with 5 m thick concrete. We have observed the background events arising from cosmic rays in 38 days and also observed the effect

from the induced events due to the high-energy particles by using vetocounters composed of plastic scintillators located up and down the target chamber. By these conditions, we have a sufficient signal to noise ratio of ten times larger than unknown fake events as listed in Table II.

Generally, there is still much debate about the screening potential which enhances the cross section for low-energy fusion reactions. Recent experiment at LUNA by Junker *et al.* [2] measured cross section of the ^{3}He(^{3}He, $2p$)^{4}He reaction at solar energies, and the data should be corrected for electron screening. For the S factor, the observed energy dependences are fitted by using four parameters $S_b(0)$, $S_b'(0)$, $S_b''(0)$, and U_e. The difference between two screening potentials, which are deduced experimentally with different fits, $U_e=432\pm29$ eV, $U_e=323\pm51$ eV, and the adiabatic limit $U_e=240$ eV remained to be not understood. Recent comprehensive instruction for this issue by Strieder and Rolfs detailed the measurement conditions for fusion reactions, stopping power at low energies and introduced the Trojan Horse method to deduce the bare $S(E)$ factor $S_b(E)$ [14]. They compared the results with the direct method for ^{7}Li(p, α)α. Recently Liolinos *et al.* derived analytical formula that establishes a lower and upper limit for the associated screening potential energy by means of the Thomas-Fermi model [15]. Despite considerable effort to reduce the ambiguity for the screening potential, the problem is not yet completely solved. We already started to study the beam-target apparatus by using an Electron Beam Ion Source as an installation for measurements for fusion cross sections among bare nuclei at low energies [16].

VI. CONCLUSION AND PERSPECTIVES

The present experiment with OCEAN has proved to reinforce the compilation data for nuclear astrophysics in solar fusion rates. A high current and low background system measured the cross section in the center of mass energy range from 50 to 30 keV. As a second series of experiments, we have started to measure at energies less than 30 keV, and these results will be reported in the near future. Better results with respect to reduced systematic and statistical errors compared to existing data are expected. When we apply a beam intensity of 1 mA for the $^3He^{2+}$ beam at $E_{\mathrm{c.m.}}=20-30$ keV and a target gas pressure of 0.1 Torr, we can expect $70-2$ events per day for real events, while the fake events will be $6-1.8$ events per day. Hence, we expect a measurement with a signal to noise ratio $10-1$ in this energy range.

ACKNOWLEDGMENTS

The authors gratefully acknowledge Professor Claus Rolfs for the design of the OCEAN accelerator facility. We acknowledge Professor T. Hasegawa for introducing ECR ion source as a bright ^{3}He particle source. We thank Dr. Uwe Greife and Dr. Mathias Junker for many suggestions to measure the reaction cross section of rare events from their experience. We thank Professor H. Ejiri, Professor Y. Nagai, and Professor H. Toki for various suggestions and discussions. We also thank Professor G. Hillhouse and Professor K. Hicks for reading critical manuscript. This work was supported by the Grant-in-Aid of Scientific Research, Ministry of Education, Science, Culture and Sports, Grant Nos. 08404015 and 0041120.

[1] U. Greife *et al.*, Nucl. Instrum. Methods Phys. Res. A **350**, 327 (1994); U. Griefe, F. Gorris, M. Junker, C. Rolfs, and D. Zahnow, Z. Phys. A **351**, 107 (1995); R. Bonetti *et al.*, Phys. Rev. Lett. **82**, 5205 (1999); H. Constantini *et al.*, Phys. Lett. B **482**, 43 (2000).

[2] M. Junker *et al.*, Phys. Rev. C **57**, 2700 (1998).

[3] A. Krauss, H. W. Becker, H. P. Trautvetter, and C. Rolfs, Nucl. Phys. **A467**, 273 (1987).

[4] R. Leroy, J. C. Angelique, P. Bertand, G. B. Blank, M. Ducourtieux, P. Foury, N. Lecesne, A. Lepine, M. Lewitowicz, C. F. Liang, J. Mandin, C. Marry, L. Maunoury, J. Mercier, J. Obert, N. A. Orr, J. Y. Pacquet, P. Paris, J. C. Potier, J. C. Putaux, E. Robert, M. G. Saint-Laurent, P. Sortais, and A. C. C. Villari, in *Proceedings of the 12th International Workshop on ECR Ion Sources, RIKEN, Japan*, internal report, edited by Masayoki Sekiguchi and Takahide Nakagawa (Institute for Nuclear Study, Tanashi, Japan, 1995), p. 57; P. Sortais, C. Bieth, P. Foury, N. Lecesne, R. Leroy, J. Mandin, C. Marry, J. Y. Pacquet, E. Robert, and A. C. C. Villari, in *Proceedings of the 12th International Workshop on ECR Ion Sources, RIKEN, Japan*, internal report, edited by Masayoki Sekiguchi and Takahide Nakagawa (Institute for Nuclear Study, Tanashi, Japan, 1995), p. 45.

[5] T. Itahashi *et al.*, Rev. Sci. Instrum. **69**, 1032 (1998); T. Itahashi *et al.*, *ibid.* **71**, 1075 (2000).

[6] A. Wollnik, WINGIOS (IONTECH), version 2.0.

[7] K. Langanke, T. D. Shoppa, C. A. Barnes and C. Rolfs, Phys. Lett. B **369**, 211 (1996).

[8] C. H. Thomann and J. E. Benn, Nucl. Instrum. Methods **138**, 293 (1976); A. E. Vlieks, M. Hilgemeier, and C. Rolfs, Nucl. Instrum. Methods Phys. Res. **213**, 291 (1983); J. M. Nitschke, *ibid.* **206**, 355 (1983).

[9] N. Kudomi *et al.*, Rev. Sci. Instrum. **72**, 2957 (2001).

[10] Y. Saitoh (private communication).

[11] J. F. Ziegler, *The Stopping and Ranges of Ions in Matter* (Pergamon Press, New York, 1985), Vol. 4.

[12] J. F. Ziegler, Program SRIM-2000, IBM Research, http://www.srim.org

[13] G. S. Chulick, Y. E. Kim, R. A. Rice, and M. Rabinowitz, Nucl. Phys. **A551**, 255 (1993).

[14] F. Strieder and C. Rolfs, Nucl. Phys. News **11**, 5 (2001).

[15] T. E. Liolinos, Phys. Rev. C **63**, 045801 (2001).

[16] T. Itahashi, N. Kudomi, E. D. Donets, and D. E. Donets, Rev. Sci. Instrum. **73**, 667 (2002).